Available online at www.sciencedirect.com
ScienceDirect
Journal of Magnetic Resonance 182 (2006) 273–282
JMR Journal of Magnetic Resonance
www.elsevier.com/locate/jmr

Dynamic nuclear polarization properties of nitroxyl radicals used in Overhauser-enhanced MRI for simultaneous molecular imaging

A. Milton Franklin Benial [1], Kazuhiro Ichikawa, Ramachandran Murugesan [2], Ken-ichi Yamada, Hideo Utsumi *

Department of Bio-functional Science, Faculty of Pharmaceutical Sciences, Kyushu University, Fukuoka 812-8582, Japan

Received 8 March 2006; revised 14 June 2006
Available online 27 July 2006

Abstract

DNP parameters relevant to Overhauser-enhanced magnetic resonance imaging (OMRI) are reported for a few nitroxyl radicals and their corresponding ^{15}N and ^{2}H enriched analogues, used in simultaneous imaging by OMRI. DNP enhancement was measured at 14.529 mT, using a custom-built scanner operating in a field-cycled mode, for different concentrations, ESR irradiation times and RF power levels. DNP enhancements increased with agent concentration up to 2.5 mM and decreased above 3 mM, in tune with ESR line broadening measured at X-band as a function of the agent concentration. The proton spin-lattice relaxation times (T_1) measured at very low Zeeman field (14.529 mT) and the longitudinal relaxivity parameters were estimated. The relaxivity parameters were in good agreement with those independently computed from the linear region of the concentration dependent enhancement. The leakage factor showed an asymptotic increase with increasing agent concentration. The coupling parameters of ^{14}N- and ^{15}N-labeled carbamoyl-PROXYL showed the interaction between the electron and nuclear spins to be mainly dipolar in origin. Upon ^{2}H labeling, about 70% and 40% increases in enhancement for ^{15}N- and ^{14}N-labeled nitroxyl agents were observed, respectively. It is envisaged that the results reported here may enable better understanding of the factors determining DNP enhancement to design suitable 'beacons' for simultaneous molecular imaging by OMRI.

Keywords: Overhauser enhancement; MRI; ESR; Redox status; Nitroxyl radical; Molecular imaging

1. Introduction

Molecular imaging is rapidly emerging as an important biomedical tool for the visual representation, characterization, and quantification of biological processes at cellular and subcellular levels [1–3]. By exploiting specific molecules as the source of image contrast, it promises new insights into disease processes. Further, the use of fewer animals in biological assays with molecular imaging is highly appealing, both on ethical as well as on economical grounds. The involvement of free radicals in a range of diseases has provoked considerable interest in the development of different modalities for free radical imaging in different laboratories [4–11]. Though ESR[3] imaging has

* Corresponding author. Fax: +81 92 642 6626.
E-mail address: utsumi@pch.phar.kyushu-u.ac.jp (H. Utsumi).
[1] Present address: JSPS Postdoctoral fellow, on leave from Department of Physics, NMSSVN College, Madurai 625 019, India.
[2] Present address: On leave from School of Chemistry, Madurai Kamaraj University, Madurai 625 021, India.

[3] *Abbreviations used:* $A_{^{14}N}$, hyperfine splitting constant for ^{14}N; B_0, Zeeman field; B_0^{ESR}, ESR Zeeman field; B_0^{NMR}, NMR Zeeman field; carboxy-PROXYL, 3-carboxy-2,2,5,5-tetramethyl-pyrrolidine-1-oxyl; carbamoyl-PROXYL, 3-carbamoyl-2,2,5,5-tetramethyl-pyrrolidine-1-oxyl; DNP, dynamic nuclear polarization; ESR, electron spin resonance; FID, free induction decay; FWHM, full-width half-maximum; GE, gradient echo; GP, gradient phase; GS, gradient slice; I, nuclear spin quantum number; MC-PROXYL, 3-methoxycarbonyl-2,2,5,5-tetramethyl-pyrrolidine-1-oxyl; m_I, nuclear spin magnetic quantum number; MRI, magnetic resonance imaging; NMR, nuclear magnetic resonance; Nrf2, NF-E2-related factor-2; OMRI, Overhauser enhanced magnetic resonance imaging; PBS, phosphate buffered solution; RF, radio frequency; ROS, reactive oxygen species; S, electron spin quantum number; T_1, proton spin-lattice relaxation time; T_E, echo time; TEMPOL, 2,2,6,6-tetramethylpiperidine-*N*-oxyl-4-ol; T_{ESR}, ESR irradiation time; T_R, repetition time.

1090-7807/$ - see front matter © 2006 Elsevier Inc. All rights reserved.
doi:10.1016/j.jmr.2006.06.025

exemplified as a sensitive and decisive free radical imaging modality, for morphological information of the radicals, it is often necessary to co-register the ESR images with MR images. Such co-registrations require additional hardware (MR imaging facility), well-thought out as well as delicate fiducial markings and suitable software for inferring the interrelated information [12]. Recently, Overhauser magnetic resonance imaging is shown to be a viable alternative to these difficulties because of the advantage that both physiologic and anatomic information can be extracted simultaneously [4–6]. OMRI is based on the Overhauser effect, wherein ESR resonance of the free-radical is irradiated during the acquisition of an MR image. Transfer of polarization from unpaired electron spins to the coupled proton spins results in the enhancement of the NMR signal in regions of the sample containing free-radical, revealing its spatial distribution in the final image. This leads to the possibility of NMR imaging at very low magnetic fields [4–6,13–16]. OMRI offers better sensitivity than the native MRI, and its spatial resolution is not limited by the line width of the free-radical, in contrast to the ESR imaging. Both the temporal and the spatial distribution of spin probes *in vivo* can be simultaneously monitored with reasonably good resolution. These advantages motivated us to explore, for the first time, the potential of OMRI for simultaneous molecular imaging of redox reactions using nitroxyl radicals [4].

Nitroxyl radicals have been widely used as spin probes for low-frequency *in vivo* ESR imaging, and as contrast agents for Overhauser imaging. Reasonable pharmacokinetic features, such as that the imaging agent reaches its intended target at sufficient concentration and remains there for sufficient time to be detectable in living subjects, are mandatory for the externally administered nitroxyl agent. Obstacles such as rapid excretion, nonspecific binding/trapping, metabolism and delivery barriers must be overcome for useful *in vivo* applications. The primary factor to be taken into account for *in vivo* imaging is the stability of the imaging agent. In this respect, the nitroxyl radical, carbamoyl-PROXYL outscores other agents to become an automatic choice for *in vivo* free radical imaging and ROS monitoring [17–22]. Carbamoyl-PROXYL has also been widely used for the evaluation of *in vivo* free radical reactions and redox status in living animals. Hepatic oxidative stress in liver, increased oxidative stress in the kidneys of diabetic mice, oxidative stress during ischemia-reperfusion in acute renal failure and the tissue-reducing activity of Nrf2 transcription factor deficient mice are a few examples that are visualized by using carbamoyl-PROXYL in conjunction with low frequency ESR imaging [23–26]. Recently, we have used ^{14}N- and ^{15}N-labeled carbamoyl-PROXYL, carboxy-PROXYL and MC-PROXYL to demonstrate the capability of OMRI to simultaneously image two different but related reactions [4]. In continuation to this work, here we report the DNP properties of these nitroxyl radicals, and their deuterated derivatives to enable us to make further improvements in the design of the nitroxyl probes, because progress in the field of simultaneous molecular imaging of redox reactions by OMRI is conditional on the construct of suitable 'beacons'.

1.1. Theory

Theoretical principles of OMRI are well documented [13–15]. Nevertheless, a brief outline of the principles relevant to the experiments reported herein is presented in this section. OMRI is based on the Overhauser effect that enhances the amplitude of the NMR signal of the solvent water protons while the ESR transition of the dissolved paramagnetic solute is saturated. The enhancement, E of the NMR signal of the ^{1}H nuclei ($I = 1/2$) of water molecules with couplings to an unpaired electron spin $S = 1/2$ of a dissolved free radical, is given by,

$$E = \frac{\langle I_Z \rangle}{I_0} = 1 - \rho f s \frac{|\gamma_e|}{\gamma_N}. \tag{1}$$

Here, $\langle I_z \rangle$ denotes the expectation value of the dynamic nuclear polarization, I_0 is its thermal equilibrium value, ρ is the coupling parameter, f is the leakage factor, s denotes the saturation parameter, and γ_e and γ_N are, respectively, the electron and nuclear gyro magnetic ratios. In native MRI, the spectral densities of the fluctuating ^{1}H–^{1}H dipolar fields, modulated by random molecular motion determine the T_1 and T_2 contrasts. For example, the differences in spectral weights at the proton Larmor frequency relate to the T_1 contrast. But, in OMRI, the spectral density function of the electron–proton interaction plays a major role. The enhancement is appreciable only when molecular motion takes place in a timescale faster than the inverse Larmor frequency of the electron spin. In the extreme narrowing limit, where the inverse electronic Larmor frequency is larger than the characteristic correlation time of the molecular motion, the coupling mechanism in most nitroxyl agents and water proton system becomes entirely dipolar in origin, and the coupling parameter ρ takes a value of 0.5, leading to maximum enhancement under the ideal conditions of 100% saturation of ESR transition and no loss of NMR polarization. But, there is a loss in polarization, brought about by the spin-lattice relaxation of nuclei within the solvent molecules via proton–proton dipolar couplings. The leakage factor f in Eq. (1) that accounts for the loss of polarization is sensitive to the motion and it depends also upon the concentration of the nitroxyl agents, as given by,

$$f = 1 - \frac{T_1}{T_{10}} = \frac{kCT_{10}}{1 + kCT_{10}}. \tag{2}$$

Here, T_1 denotes the NMR spin-lattice relaxation time of the water protons of the nitroxyl agent solution. Intrinsic nuclear relaxation rate of water protons in the absence of nitroxyl agent is denoted by $1/T_{10}$. The concentration of the nitroxyl agent is given by C, and k denotes the relaxivity constant. As the concentration of the agents is increased

the leakage factor approaches to unity, because with increasing C, $kC \gg 1/T_{10}$.

The factor more critical to the sensitivity of OMRI is given by the degree of saturation of the electron spin,

$$s = \frac{(S_0 - \langle S_Z \rangle)}{S_0}, \tag{3}$$

which at a given ESR power, depends on the electron spin relaxation rates of the nitroxyl agent. For on resonance irradiation at the center frequency of one of the hyperfine components of the nitroxyl agent, by an oscillating magnetic field of amplitude B_1, the saturation factor is given by,

$$s = \frac{\gamma_e^2 B_1^2 T_{1e} T_{2e}}{1 + \gamma_e^2 B_1^2 T_{1e} T_{2e}}. \tag{4}$$

Here, T_{1e} and T_{2e} are the electron spin–lattice and spin–spin relaxation times, respectively. The transverse relaxation rate, given by,

$$\frac{1}{T_{2e}} = \frac{1}{T_{2e}^{|}} + \frac{1}{T_{1e}^{|}} \tag{5}$$

contains a secular term $1/T_{2e}^{|}$ and a lifetime broadening, nonsecular term $1/T_{1e}^{|}$. For small free radical concentration and low viscosity, both $1/T_{2e}^{|} + 1/T_{1e}^{|}$ are often dominated by motion-induced modulation of intramolecular anisotropic interactions, and the saturation parameter, s is expected to be independent of free radical concentration. Under such condition the enhancement factor is mainly determined by Eq. (2). Hence, in this regime a plot of $1/(1 - E)$ vs. $1/C$ is expected to be linear. But as the concentration of the nitroxyl agent is further increased, the interaction between the radicals dominates, leading to line broadening, and consequently to reduced saturation factor at a given RF power level. For complete saturation of one of the ESR transitions, and the condition that $1/T_{10} \ll 1/T_1$, the enhancement factor is given by,

$$1 - E = -\frac{(\gamma_e/\gamma_N)\rho}{(2I+1)}, \tag{6}$$

where I is the relevant nuclear spin quantum number, (1 for ^{14}N and 1/2 for ^{15}N). The Overhauser enhancement reaches maximum values of 110 and 165, respectively, for ^{14}N and ^{15}N nitroxyl agents for pure dipolar, and 220 and 330 for scalar interactions. Experimentally, these maximum values are not realized due to many factors. In nitroxyl agents, there is additional hyperfine interaction between the hydrogen nuclei and the unpaired electron. Hence the three (for ^{14}N) or two (for ^{15}N) ESR lines are inhomogeneously broadened due to the presence of the unresolved hydrogen hyperfine. An inhomogeneously broadened ESR line with very closely spaced hyperfine lines has Voigt line shape function, the convolution of a Lorentzian line shape with a Gaussian intensity profile [16]. Hence, Eq. (4) will no longer hold good, and irradiation of one of the nitrogen hyperfine lines will result only in partial saturation. Nevertheless, the enhancement factor, achieved by irradiating a single ESR line of the nitrogen hyperfine line of the nitroxyl agent can be approximately given [14,15] by combining Eqs. (1), (2) and (6),

$$\frac{1}{1-E} = \frac{1}{658}\left(1 + \frac{1}{kCT_{10}}\right)(2I+1)\left(1 + \frac{1}{\alpha P}\right)\frac{1}{\rho}. \tag{7}$$

Here, P is the applied ESR power level, which is proportional to B_1^2, and α is a constant related to the conversion efficiency of the coil and the relaxation times of the electron spins. Therefore, a plot of reciprocal enhancement against reciprocal power, $1/P$, should give a straight line with intercept $1/(1 - E_{max})$ where E_{max} is the maximum enhancement achieved under complete saturation of the ESR signal. The effect of concentration on the enhancement factor can be better visualized by rearranging Eq. (7) as

$$\frac{s}{1-E} = \frac{1}{658}\left(1 + \frac{1}{kCT_{10}}\right)\frac{1}{\rho}, \tag{8}$$

where $s = [1/(2I+1)] \times \alpha P/(1 + \alpha P)$. Therefore, a plot of $s/(1 - E)$ against $1/C$ should be linear and the slope must be consistent with the independently determined kT_{10}. The intercept of the low concentration region, linear portion of $s/(1 - E)$ extrapolated to $1/C = 0$, can thus provide an additional check of the experimental data.

2. Materials and methods

The spin probes, carboxy-PROXYL, carbamoyl-PROXYL were purchased from Aldrich Chemical Co, St. Louis, MO, USA. MC-PROXYL was synthesized as described earlier [27]. ^{15}N-Labeled nitroxyl probes were synthesized in our laboratory by using ^{15}N-ammonium chloride (Cambridge Isotope Laboratories, Inc. MA, USA) as per literature [28]. ^{15}N-Labeled deuterated nitroxyl probes were synthesized by using ^{15}N-ammonium chloride and deuterated acetone. Any contamination of ^{14}N was ruled out by ESR spectroscopy. All other chemicals used were of commercially available reagent grade quality.

The DNP experiments were performed on a custom-built (Philips Research Laboratories, Hamburg, Germany), human whole-body (Magnet bore: 79 cm diameter; 125 cm length), low field (14.529 mT) scanner operating in a field-cycled mode to avoid excess RF power deposition during the ESR cycle [29]. The B_0^{ESR} was set at 6.089 and 6.569 mT for ^{14}N- and ^{15}N-labeled nitroxyl radical, respectively, and the B_0^{NMR} was set at 14.529 mT. The ESR irradiation frequency used was 220.6 MHz. A saddle coil (13.5 cm diameter, 23.5 cm length) was used as the ESR resonator. The efficiency parameter of the ESR coil used was measured to be 5.2 $\mu T/W^{1/2}$. The NMR resonator assembly consisting of a transmit saddle coil (25 cm diameter, 23 cm length) and a receive solenoidal coil (5 cm diameter, 6 cm length) was tuned to 617 kHz with a band width of 1.5 kHz. The phantoms employed in the DNP experiments were 2 cm diameter tubes filled with 10 ml of nitroxyl radical solutions of various

concentrations in water. The phantom tubes were placed vertically in the solenoidal receive coil.

DNP spectra of 2 mM aqueous solutions of ^{14}N- and ^{15}N-labeled carbamoyl-PROXYL were recorded by sweeping the magnetic field (B_0^{ESR}) from 5 to 10 mT, in steps of 0.1 mT, while away from the resonance and in steps of 0.01 mT, while near the resonance for better peak identification using ESR irradiation time (T_{ESR}), 800 ms and power, 53.8 W. ESR line width measurements for various concentrations of nitroxyl radicals in water were carried out with an accuracy of $\sim\pm0.5$ μT using an X-band ESR spectrometer (JEOL Co. Ltd., Akishima, Tokyo, Japan).

Imaging experiments were performed by using standard spin warp gradient echo sequence for MRI, except that each phase encoding step was preceded by an ESR saturation pulse to elicit the Overhauser enhancement (Fig. 1). The pulse sequence started with the ramping of the B_0 field to 6.089 mT for ^{14}N-labeled nitroxyl radical or 6.569 mT for ^{15}N-labeled nitroxyl radical, followed by switching on the ESR irradiation. Then, the B_0 was ramped up to 14.529 mT before the NMR pulse (617 kHz) and the associated field gradients were turned on. At the beginning or end of the cycle, a conventional (native) NMR signal intensity (with ESR OFF) was measured for computing the enhancement factors. A Hewlett-Packard PC (operating system, LINUX 5.2) was used for data acquisition. The images were reconstructed from the echoes by using standard software, and were stored in DICOM format (Digital Imaging and Communications in Medicine). MATLAB codes were used for the computation of DNP parameters and curve fitting. The reproducibility of the data was confirmed with several experiments, and fitted parameters and enhancement factors which were obtained from one of the data set showed good correlation ($R^2 > 0.999$). Typical scan conditions were as follows, repetition time (T_R)/echo time (T_E): 2000 ms/25 ms; ESR irradiation time (T_{ESR}): $50 \sim 800$ ms, in steps of 50 or 100 ms; ESR power, 53.8 W; no. of averages, 10; phase encoding steps, 64 and slice thickness, 20 mm. The image field of view (48 mm) was represented by a 64×64 matrix, with a pixel size of 0.63 mm × 0.63 mm.

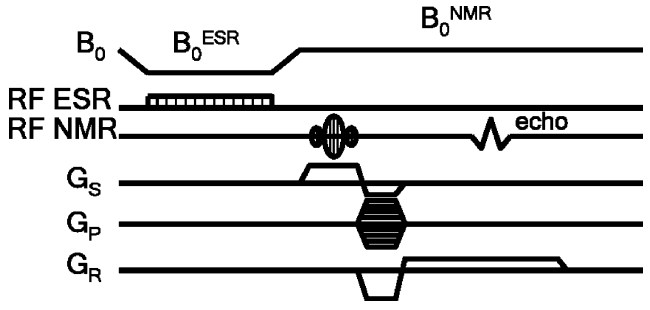

Fig. 1. Field-cycled OMRI pulse sequence starts with the ramping of the B_0^{ESR} field to 6.089 mT for ^{14}N-labeled nitroxyl radical or 6.569 mT for ^{15}N-labeled nitroxyl radical, followed by switching on the ESR irradiation, (220.6 MHz). The B_0 is ramped up to 14.529 mT before the NMR pulse and the associated field gradients are turned on. The field settling time was set at 18 ms.

3. Results and discussion

3.1. DNP spectra

To find the optimal resonance conditions for ESR excitation in the OMRI experiments, field-cycled DNP spectra of aqueous solutions of ^{14}N- and ^{15}N-labeled carbamoyl-PROXYL were measured at 23 °C by field-cycled DNP spectroscopy, by irradiating at a fixed ESR frequency (220.6 MHz) while sweeping the magnetic field to cover each resonance. When an ESR resonance is encountered, the Overhauser effect causes an enhancement of the NMR signal, and its amplitude is altered. Therefore, a plot of NMR signal amplitude versus B_0^{ESR} shows the positions of the ESR resonances. The relative amplitudes of the peaks (or, more usually troughs) provide information on the ESR line intensities, modulated by the electron–proton coupling. field-cycled DNP spectra (Fig. 2) were collected with a field sweep of 5 mT both for ^{14}N and ^{15}N, centered on 7.5 mT using the field-cycled DNP pulse sequence given in Fig. 1. The DNP spectra show three hyperfine lines for ^{14}N and two for ^{15}N-labeled carbamoyl-PROXYL. The position of the peaks and the FWHM of each line are listed in Table 1. A small m_I dependent line width and second-order effects in hyperfine splitting were observed. While isotopic substitution is not expected to affect the g-factor,

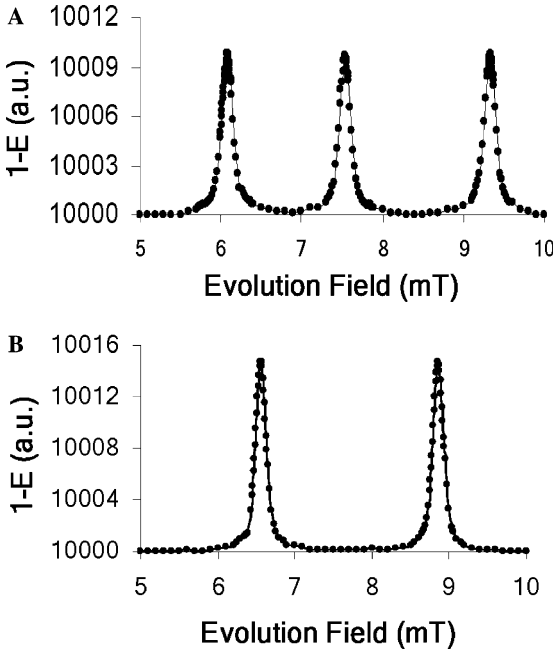

Fig. 2. Field-cycled DNP spectra of 2 mM aqueous solution of (A) ^{14}N- and (B) ^{15}N-labeled carbamoyl-PROXYL. Pulse sequence parameters: $T_R/T_{ESR}/T_E$, 2000 ms/800 ms/25 ms; no. of averages, 2; other scan parameters are as given under Section 2.

Table 1
Peak positions and FWHM of DNP spectra of ^{14}N- and ^{15}N-labeled carbamoyl-PROXYL

Nitroxyl radical	Peak position (mT)			FWHM (μT)		
	Low frequency	Middle frequency	High frequency	Low frequency	Middle frequency	High frequency
^{14}N carbamoyl-PROXYL	6.092 (335.3)	7.542 (336.9)	9.337 (338.5)	120 (116.4)	115 (117.5)	130 (121.2)
^{15}N carbamoyl-PROXYL	6.570 (335.8)	—	8.865 (338.0)	120 (111.2)	—	120 (111.2)

X-band ESR spectral data are given inside the parentheses.

the hyperfine values are expected to change in accordance with the γ of the nuclei. Thus, the hyperfine coupling of ^{15}N is expected to be about 1.4 times that of ^{14}N based on the nuclear gyro-magnetic ratio [30]. Using an average value for the observed A_N^{14} the experimentally observed ratio was computed to be 1.41.

In the pulse sequence employed in the OMRI experiments, a saturating ESR pulse of duration T_{ESR} is applied preceding the NMR pulse. After switching on the ESR irradiation the nuclear polarization builds up at a rate governed by the NMR longitudinal relaxation time, T_1. To achieve the maximum possible Overhauser enhancement, it is necessary to irradiate the ESR transition of the nitroxyl agent for at least $3T_1$. But at high power, long T_{ESR} is an undesirable option for *in vivo* studies. Short T_{ESR} not only minimizes the heating effects but also reduces unwanted RF interference and hence limits the instrumental noise. Therefore, in the selection of T_{ESR} an optimal compromise needs to be made between the signal enhancement and the RF heating. Hence to arrive at optimal T_{ESR}, the enhancement factors were measured as a function of T_{ESR} for a moderate power of 53.8 W for various concentration of the nitroxyl agent. These results, plotted in Fig. 3 show increasing signal enhancement with increasing T_{ESR}. However, for $T_{ESR} > 600$ ms, the increase in enhancement was not significant enough to offset the disadvantage of RF heating. Therefore, $T_{ESR} = 600$ ms was selected as an optimal compromise for the imaging experiments.

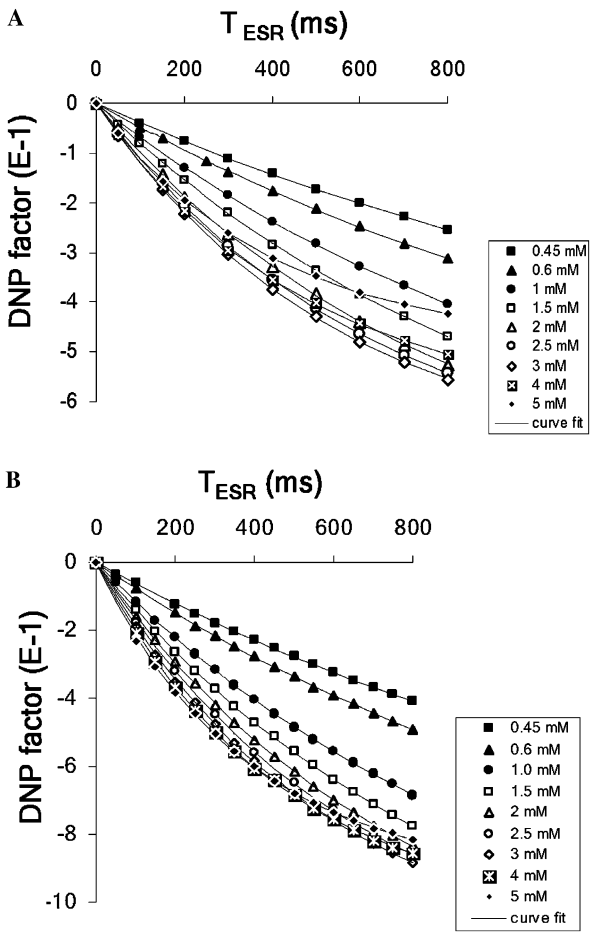

Fig. 3. Illustration of the effect of T_{ESR} on the DNP enhancement of (A) ^{14}N- and (B) ^{15}N-labeled carbamoyl-PROXYL of various concentrations. The solid lines correspond to an exponential decay curve fit to Eq. (9). Scan parameters are as given in Section 2.

3.2. Concentration dependence of enhancement factor

To determine the optimal nitroxyl radical concentration for imaging, the enhancement factors were measured as a function of various nitroxyl agent concentrations ranging from 0.45 to 5 mM by irradiating at the low field ESR line of ^{14}N as well as ^{15}N-labeled carbamoyl-PROXYL. The enhancement values were negative as usually reported in the DNP literature that takes account of the 180° phase shift of the FID when DNP occurs. The results, plotted in Fig. 4 show an increase in enhancement up to a concentration of about 2.5 mM. A linear relationship between $1/(1-E)$ and $1/C$ was observed in this range, as predicted by Eq. (7). However, with further increase in concentration, the enhancement factor no longer increased; instead it reached a plateau at 2.5–3 mM, and then started declining above 3 mM. At higher concentrations, it is likely that dipolar and spin-exchange interactions can broaden the ESR resonance, resulting in a decrease in saturation of the electron spin system for a given applied power, compared to that at lower concentrations, which in turn will reduce the OMRI signal enhancement. The decrease in enhancement above 3 mM is greater for ^{14}N, perhaps due to the greater line broadening possible for the quadrupolar ^{14}N nucleus.

3.3. T_1 relaxivity and enhancement

Eqs. (2) and (7) indicate the effect of free radical concentration on the enhancement factor. Eq. (2) reveals that the

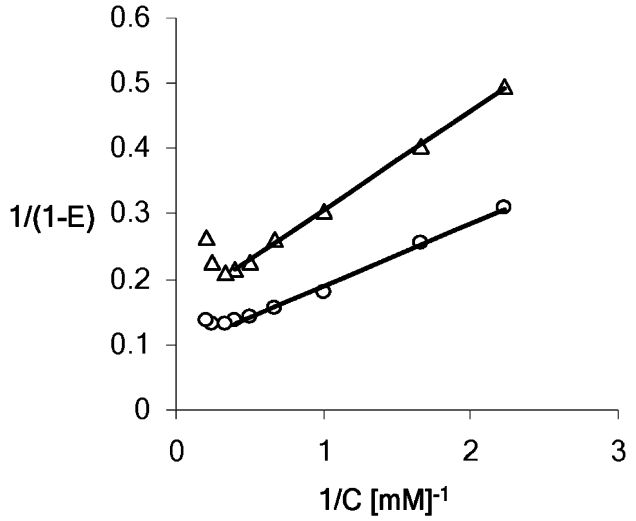

Fig. 4. Concentration dependence of the DNP enhancement for aqueous solutions of ^{14}N (Δ) and ^{15}N (○) labeled carbamoyl-PROXYL. Pulse sequence parameters: $T_R/T_{ESR}/T_E$, 2000 ms/600 ms/25 ms; no. of averages, 10; other scan parameters are as given under Section 2. The solid line represents a linear fit to Eq. (7).

concentration dependence is via the leakage factor where the longitudinal NMR relaxivity (k) of the nitroxyl radical plays a significant role. The DNP factor is proportional to the free radical concentration as long as the concentration is low enough to cause any line broadening. Hence, it would be of interest to estimate the relaxivity, k from the concentration-dependent enhancement. It is readily seen from Eq. (7) that from the slope and intercept of the linear region of the plot (Fig. 4), kT_{10} can be computed. The computed kT_{10} values 1.01 and 0.97 mM^{-1} for ^{14}N- and ^{15}N-labeled carbamoyl-PROXYL are nearly the same, but are about 40% less than that of TEMPOL [14].

Another factor that affects the build up and decay of the polarization of water protons is the NMR T_1. Following the ESR irradiation, it is necessary to ramp up the magnetic field from the evolution field (6.089/6.569 mT) to the detection field (14.529 mT) in a time that is short compared to the sample's T_1. Hence, it would be of interest to analyze how T_1 is affected by the free radical concentration. While it is straightforward to determine proton T_1 values at high Zeeman fields using standard pulse sequences, such measurements are not practical because of the poor native (unenhanced) NMR sensitivity at the very low Zeeman field (14.529 mT) used in OMRI. To alleviate this problem, a simple method for proton T_1 measurement, using OMRI has been recently reported [31]. This method is based on fitting the enhancement factors as a function of T_{ESR} using the equation [31,32].

$$E - 1 = (E_{inf} - 1) \times (1 - \exp^{-\frac{T_{ESR}}{T_1}}). \quad (9)$$

Here, E is the Overhauser enhancement factor, and E_{inf} is the theoretical maximum enhancement factor corrected for the actual T_1. Hence, DNP enhancement was measured as a function of T_{ESR} for ^{14}N- and ^{15}N-labeled carbamoyl-PROXYL in water for various concentrations and these results are presented in Fig. 3. By curve fitting the observed enhancement factors to Eq. (9), the NMR spin-lattice relaxation time for different concentrations of the free radical solutions was computed. The proton spin-lattice relaxation rate thus calculated (Fig. 5) showed an increase with increasing agent concentration. The change in the enhancement factors brought about by the different concentration may arise from the different proton T_1 values or different saturation factor brought about by the ESR line broadening. However, X-band ESR linewidth measurements (given in Fig. 6), showed very small ESR line broadening was observed at radical concentration up to 2.5 mM and caused

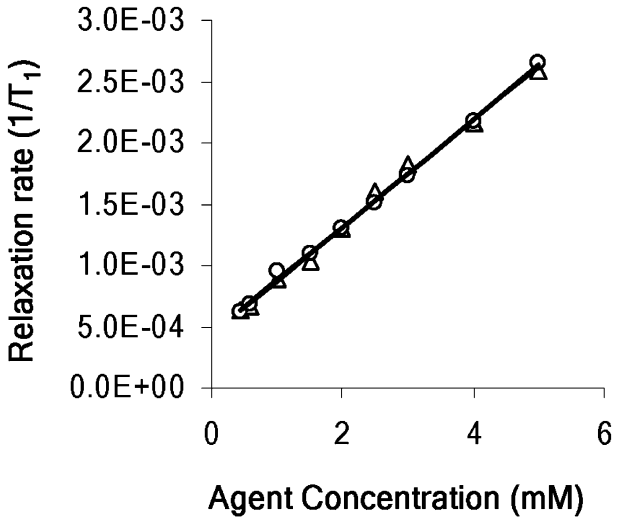

Fig. 5. The water proton longitudinal relaxation rate as a function of concentration for ^{14}N (Δ) and ^{15}N (○) labeled carbamoyl-PROXYL solutions. The solid line indicates a linear fit to Eq. (2).

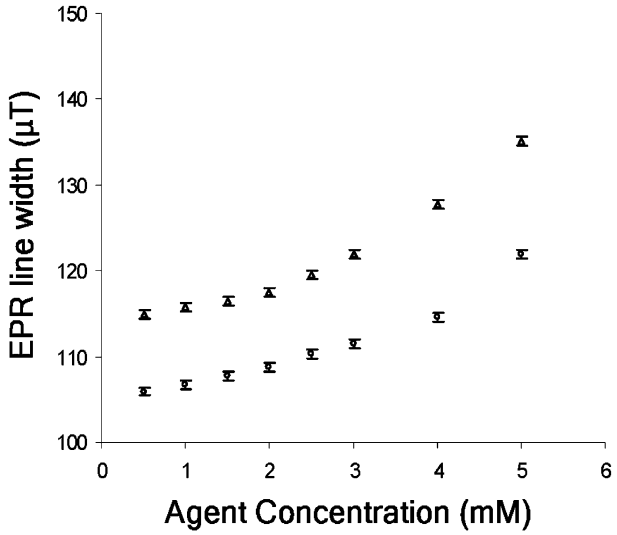

Fig. 6. X-band ESR line width measured as a function of concentration for ^{14}N (Δ) and ^{15}N (○) labeled carbamoyl-PROXYL solutions. The ESR line width of nitroxyl radical is generally larger for the quadrupolar ^{14}N system.

little change in the saturation factor. A plot of solvent proton relaxation rate, $1/T_1$ against the agent concentration is linear as expected from Eq. (2). From the linear fit (Fig. 5), the longitudinal relaxivities (k) of the nitroxyl radicals were calculated from the slope and are given in Table 2. The proton spin-lattice relaxation time at zero radical concentration (T_{10}) was computed from the intercept (Fig. 5). These values 2311 and 2287 ms for ^{14}N- and ^{15}N-labeled carbamoyl-PROXYL, respectively, compare well with the reported value of 2650 ms measured at 16 mT [15], thus validating the accuracy of the experimental procedure. Additional support for experimental consistency comes from the fact that the kT_{10} values, thus computed from T_1 relaxation time measurements agree well with the value obtained earlier, independently from the intercept and slope of the linear region of the plot (Fig. 4) and as predicted by Eqs. (7) and (8).

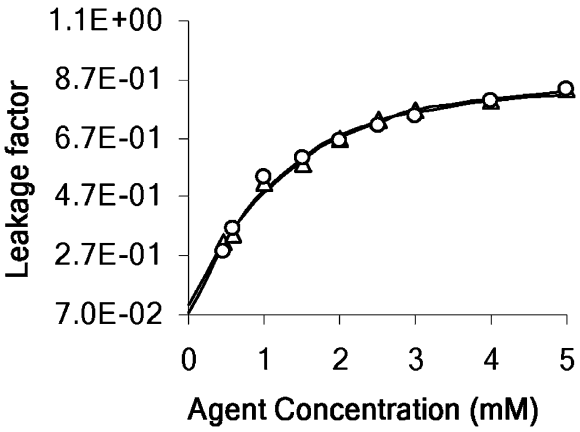

Fig. 7. Concentration dependence of the leakage factor for ^{14}N (Δ) and ^{15}N (○) labeled carbamoyl-PROXYL in aqueous solutions. The solid line corresponds to an exponential growth curve fit.

3.4. Leakage factor

The computation of T_{10} and the longitudinal relaxivity k now enables to estimate the leakage factor (f) for the nitroxyl radicals at different concentrations. The leakage factors thus computed for ^{14}N carbamoyl-PROXYL and ^{15}N carbamoyl-PROXYL as a function of concentration are plotted in Fig. 7. The leakage factor, f measures the fraction of the total relaxation rate due to nuclear–electron interactions. For weak interactions, f approaches zero and when the interactions are dominant, $f = 1$. Fig. 7 reveals that the leakage factor increases asymptotically approaching unity, as the concentration of the agent is increased. However, it is evident that above 2.5 mM the increase in f is not very significant. Above 2.5 mM, the line broadening will also offset any gain achieved from the increased 'f' value. Hence, the leakage parameter also points out to an optimal concentration range of 2–2.5 mM.

3.5. Saturation parameter

Complete saturation of one of the ESR lines cannot generally be achieved directly. According to the Bloch equation the reciprocal of the spin polarization ($\langle S\rangle^{-1}$) is proportional to the reciprocal of the ESR irradiation power (P^{-1}). The saturation parameters (s) can be determined, for a given concentration by measuring the enhancement as a function of applied RF power. The intercept of a plot of $1/(1-E)$ against $1/P$ can be used to estimate E_{max}, the enhancement factor at complete ESR saturation, which characterizes the overall interaction of the free radicals with the solvent water molecules. In addition, E_{max} also enables to compare the enhancement efficiency of different nitroxyl agents without being biased by instrumental parameters such as resonator Q-factor, RF power, T_{ESR} etc. Hence, enhancements at various power levels were measured for 2 mM aqueous solutions of ^{14}N- and ^{15}N-labeled carbamoyl-PROXYL. These results, plotted in Fig. 8 as reciprocal enhancement $1/(1-E)$, against reciprocal power, $1/P$, give a linear relationship according to the Eq. (8). Therefore, from Fig. 8, on extrapolation to $1/P = 0$, the E_{max} values were computed to be −64.4 and −100 for 2 mM solutions of ^{14}N- and ^{15}N-labeled carbamoyl-PROXYL, respectively. For this investigation, a huge power level of up to 152.8 W was used to make the extrapolation more accurate. It would be of interest to investigate the saturation factor at the RF power level used for *in vivo* studies [4]. This can be readily achieved by computing the ratio of $1/(1-E)$ at the power opted for *in vivo* studies. For 2 mM solutions of ^{14}N- and ^{15}N-labeled

Table 2
The DNP parameters of various nitroxyl radicals

Nitroxyl radical	Solvent	ΔB_{pp}[a] (μT)	k (mM s)$^{-1}$	E_{max}[b]	f	ρ	B_0 (mT)		kT_{10} from		Ref.
							ESR	NMR	T_1 measurement	Concentration dependent enhancement	
^{14}N carbamoyl-PROXYL	Water	116.4	0.44	−64.4	0.67	0.45	6.089	14.529	1.02	1.01	This work
^{15}N carbamoyl-PROXYL	Water	111.2	0.44	−100.0	0.67	0.46	6.569	14.529	1.00	0.97	This work
^{14}N carbamoyl-PROXYL	PBS	112	0.57	−31.3	0.70	0.21	6.751	6.751	—	—	[33]
TEMPOL	PBS	151	0.66	−40.5	0.73	0.26	6.751	6.751	—	—	[33]
TEMPOL	Water	—	—	—	—	0.57	10.0	10.0	1.42	1.45	[14]

[a] X-band, peak to peak line width.
[b] E_{max} is the extrapolated enhancement factor at complete saturation measured for 2 mM concentration.

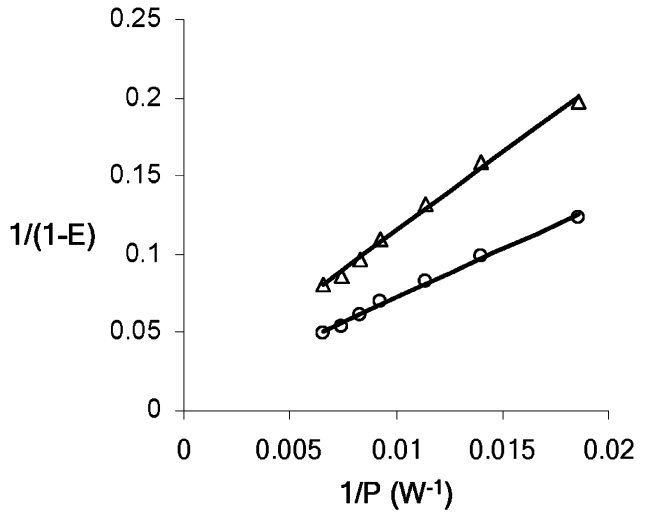

Fig. 8. Effect of ESR irradiation power on the enhancement for 2 mM aqueous solution of ^{14}N (Δ) and ^{15}N (○) labeled carbamoyl-PROXYL in aqueous solution. The ESR power varied from 53.8 to 152.8 W for ESR irradiation time, 800 ms; other scan parameters are as given in Section 2. The solid line represents a linear fit to Eq. (7).

carbamoyl-PROXYL, the saturation factors at 53.8 W were thus computed to be 0.023 and 0.037, respectively. The low values of saturation parameter (s) indicate that in the design of suitable agents for OMRI, importance must be given to factors that can enhance the saturation parameter (s) significantly.

3.6. Coupling factor

In dilute solutions of nitroxyl agents the rapid diffusion of the solute ensures that all nuclei are equally affected. Hence the nuclear relaxation is often dominated by the pair wise interactions between the unpaired electron and the nuclei. The strong local fields produced by the electron can be coupled to the nuclei by a dipole–dipole interaction and sometimes coupling by scalar interaction is also possible. Measurement of coupling parameter ρ (Eq. (1)) can throw light on the mechanism of coupling. The measurement of E_{max} enables the computation of ρ from Eq. (1). The ρ values thus calculated were 0.45 and 0.46 for ^{14}N- and ^{15}N-labeled carbamoyl-PROXYL, respectively. These values are in support of the dipolar interaction as the major mechanism of coupling between the electron spin with the nuclear spin, as observed in many other nitroxyl agents [14,33].

3.7. ^{2}H-substituted nitroxyl agents

Major limitations that hinder the development of OMRI as a simultaneous molecular imaging tool for biomedical application are the sensitivity of detection and RF-tissue heating. These two problems can be, to some extent alleviated by designing nitroxyl radicals with very small line width. In our laboratory, we have been focusing on the development of spin probes for site-specific imaging of redox-status or ROS generation at intra- and extracellular locations [18,34,35]. Hence, line width reduction in these nitroxyl agents for enhancing their potential as simultaneous molecular imaging agent in OMRI was investigated by deuterium substitution. In addition to the line width reduction, there are two more added advantages upon ^{2}H labeling. The deuterated nitroxyl agents are known to exhibit nearly homogeneous line width whereas the corresponding protonated spin probes exhibit substantial inhomogeneity [36,37]. For inhomogeneous lines, the hypothesis of single electron Zeeman spin temperature is not valid. The RF irradiation results in hole-burning rather than uniform excitation. Although the electron-electron cross relaxation across the inhomogenously broadened ESR line can render the line homogeneous over sufficiently long time scales, at low concentrations more power is needed to saturate the homogeneous line width. ^{2}H substitution can reduce the width of the ESR lines, because of the lower magnetic moment of deuterium (compared to that of the proton). Analysis of line width data given in Table 3, shows that the ^{15}N substitution does not significantly reduce the line width, whereas the line width reduction is significant for ^{2}H labeling.

The saturation of a resonance line depends on the power of the RF field and on the relaxation times of the free electrons. Therefore, the same electron resonance saturation can be obtained for a deuterium substituted nitroxyl radical as that of ^{1}H nitroxyl radical, but with less RF power. This is a good way to decrease the RF-heating of *in vivo* samples during ESR irradiation in OMRI. Alternatively, the advantage of increase in signal intensity for the same level of power can be used to reduce the toxicity by reducing the dose of the nitroxyl agent. Another factor to be considered in *in vivo* studies is the three spin effect. The biological system is not a homogeneous proton system. Instead it consists of water protons, protein protons, and lipid protons. The DNP

Table 3
Comparison of the DNP enhancement factors and X-band ESR line widths of low field line for different nitroxyl radicals

Nitroxyl radical	DNP enhancement factor				ESR line width (μT)			
	^{14}N,H	^{14}N,D	^{15}N,H	^{15}N,D	^{14}N,H	^{14}N,D	^{15}N,H	^{15}N,D
Carbamoyl-PROXYL	−5.26	−7.44	−8.31	−13.58	116.4	78.0	111.2	70.3
Carboxy-PROXYL	−5.06	−7.32	−8.06	−14.18	115.2	77.3	113.1	70.7
MC-PROXYL	−5.08	−7.21	−7.94	−13.69	115.5	79.1	110.2	71.0

enhancement will in principle depend on the transfer of magnetization between these proton systems. Protein binding can quench the DNP enhancement. Therefore, the deuterated nitroxyl agents will have the additional advantage of low *in vivo* toxicity and reduced quenching of DNP enhancement. Hence, DNP enhancement measurements were carried out for 2 mM aqueous solutions ^{2}H-labeled ^{14}N and ^{15}N carbamoyl-PROXYL, carboxy-PROXYL, and MC-PROXYL. These values, listed in Table 3 show increase of enhancement of about 70% and 40% for ^{15}N- and ^{14}N-labeled nitroxyl agents, respectively, upon ^{2}H labeling.

4. Conclusions

The objective of this study was to investigate the DNP properties of ^{14}N and ^{15}N substituted carbamoyl-PROXYL, carboxy-PROXYL and MC-PROXYL and their deuterated derivatives to assess their use as molecular imaging probes in OMRI. The rationale for the selection of these agents were that (i) they have relatively long *in vivo* stability, (ii) in combination they can be used as probes for simultaneously monitoring inter- and intracellular redox status, if one of them is labeled with ^{15}N. The measurement of DNP parameters that govern the water proton signal enhancement can provide guideline for further enhancing their utility as simultaneous molecular imaging agent in OMRI. We have measured Overhauser enhancement over a wide range of concentration, saturating RF power level and RF irradiation time completely to assess the various DNP properties such as longitudinal relaxivity, saturation parameter, leakage factor, coupling factor etc. The ^{15}N substitution increases the signal intensity, because the saturation of one ESR line in ^{15}N nitroxyl radical induces a 17% (50–33%) increase in the proton polarization. Similarly, the significant increase in enhancement for ^{14}N- and ^{15}N-labeled nitroxyl agents, upon ^{2}H substitution strongly recommends ^{2}H labeling of both the agents.

Acknowledgments

This work was supported by Grants-in-Aid for Scientific Research (A) from Japan Society for the Promotion of Science (JSPS), Grants-in-Aid for Scientific Research on Priority Areas "Application of Molecular Spins" and 21st Century Centers of Excellence (COE) program of Kyushu University from the Ministry of Education, Culture, Sports, Science and Technology of Japan. This work was also supported by "Development of System and Technology for Advanced Measurement and Analysis" from Japan Science and Technology Agency. One of the authors (A. Milton Franklin Benial) is a Postdoctoral Fellow for Foreign Researchers (ID No. P 04489) supported by the Grant-in-Aid for JSPS, and thanks NMSSVN College, Madurai-625 019, India for encouragement and leave for postdoctoral research studies.

References

[1] R. Weissleder, U. Mahmood, Molecular imaging, Radiology 219 (2001) 316–333.
[2] I.J. Hildebrandt, S.S. Gambhir, Molecular imaging applications for immunology, Clin. Immunol. 111 (2004) 210–224.
[3] T.F. Massoud, S.S. Gambhir, Molecular imaging in living subjects: seeing fundamental biological processes in a new light, Genes Dev. 17 (2003) 545–580.
[4] H. Utsumi, K. Yamada, K. Ichikawa, K. Sakai, Y. Kinoshita, S. Matsumoto, M. Nagai, Simultaneous molecular imaging of redox reactions monitored by Overhauser-enhanced MRI with ^{14}N- and ^{15}N-labeled nitroxyl radicals, Proc. Natl. Acad. Sci. USA 103 (2006) 1463–1468.
[5] M.C. Krishna, S. English, K. Yamada, J. Yoo, R. Murugesan, N. Devasahayam, J.A. Cook, K. Golman, J.H. Ardenkjaer-Larsen, S. Subramanian, J.B. Mitchell, Overhauser enhanced magnetic resonance imaging for tumor oximetry: coregistration of tumor anatomy and tissue oxygen concentration, Proc. Natl. Acad. Sci. USA 99 (2002) 2216–2221.
[6] R. Murugesan, S. English, K. Reijnders, K. Yamada, J.A. Cook, J.B. Mitchell, S. Subramanian, M.C. Krishna, Fluorine electron double resonance imaging for ^{19}F MRI in low magnetic fields, Magn. Reson. Med. 48 (2002) 523–529.
[7] H. Li, Y. Deng, G. He, P. Kuppusamy, D.J. Lurie, J.L. Zweier, Proton electron double resonance imaging of the *in vivo* distribution and clearance of a triaryl methyl radical in mice, Magn. Reson. Med. 48 (2002) 530–534.
[8] M. Elas, B.B. Williams, A. Parasca, C. Mailer, C.A. Pelizzari, M.A. Lewis, J.N. River, G.S. Karczmar, E.D. Barth, H.J. Halpern, Quantitative tumor oxymetric images from 4D electron paramagnetic resonance imaging (EPRI): methodology and comparison with blood oxygen level-dependent (BOLD) MRI, Magn. Reson. Med. 49 (2003) 682–691.
[9] S.S. Eaton, G.R. Eaton, ESR imaging, in: C.P. Pool, H.A. Farach (Eds.), Handbook of Electron Spin Resonance, AIP Press/Springer, New York, 1999, pp. 327–343.
[10] P. Kuppusamy, J.L. Chzhan, J.L. Zweier, Principles of imaging, in: L.J. Berlinear (Ed.), *In vivo* EPR(ESR) Theory and application, Kluwer Academic/Plenum Publishers, New York, 2003, pp. 99–152.
[11] N. Nestle, K. Shet, D.J. Lurie, Proton electron double resonance imaging of free radical distribution in environmental science applications—first results and perspectives, Magn. Reson. Imaging 23 (2005) 183–189.
[12] S. Matsumoto, M. Nagai, K. Yamada, F. Hyodo, K. Yasukawa, M. Muraoka, H. Hirata, M. Ono, H. Utsumi, A composite resonator assembly suitable for EPR/NMR coregistration imaging, Concepts Magn. Reson. Part B 25B (2005) 1–11.
[13] T. Guiberteau, D. Grucker, EPR spectroscopy by dynamic nuclear polarization in low magnetic field, J. Magn. Reson. Ser. B 110 (1996) 47–54.
[14] I. Nicholson, D.J. Lurie, F.J.L. Robb, The application of proton–electron double-resonance imaging techniques to proton mobility studies, J. Magn. Reson. Ser. B 104 (1994) 250–255.
[15] P.L. de Sousa, R.E. de Souza, M. Engelsberg, L.A. Colnago, Mobility and free radical concentration effects in proton-electron double-resonance imaging, J. Magn. Reson. 135 (1998) 118–125.
[16] J.H. Ardenkjaer-Larsen, I. Laursen, I. Leunbach, G. Ehnholm, L.G. Wistrand, J.S. Petersson, K. Golman, EPR and DNP properties of certain novel single electron contrast agents intended for oxymetric imaging, J. Magn. Reson. 133 (1998) 1–12.
[17] K. Matsumoto, M.C. Krishna, J.B. Mitchell, Novel pharmacokinetic measurement using electron paramagnetic resonance spectroscopy and simulation of *in vivo* decay of various nitroxyl spin probes in mouse blood, J. Pharmacol. Exp. Ther. 310 (2004) 1076–1083.

[18] M. Yamato, T. Egashira, H. Utsumi, Application of *in vivo* ESR spectroscopy to measurement of cerebrovascular ROS generation in stroke, Free Radic. Biol. Med. 35 (2003) 1619–1631.
[19] T. Sano, F. Umeda, T. Hashimoto, H. Nawata, H. Utsumi, Oxidative stress measurement by *in vivo* electron spin resonance spectroscopy in rats with streptozotocin-induced diabetes, Diabetologia 41 (1998) 1355–1360.
[20] N. Phumala, T. Ide, H. Utsumi, Noninvasive evaluation of *in vivo* free radical reactions catalyzed by iron using *in vivo* ESR spectroscopy, Free Radic. Biol. Med. 26 (1999) 1209–1217.
[21] K. Kasazaki, K. Yasukawa, H. Sano, H. Utsumi, Non-invasive analysis of reactive oxygen species generated in NH_4OH-induced gastric lesions of rats using a 300 MHz *in vivo* ESR technique, Free Radic. Res. 37 (2003) 757–766.
[22] K. Yasukawa, K. Kasazaki, F. Hyodo, H. Utsumi, Non-invasive analysis of reactive oxygen species generated in rats with water immersion restraint-induced gastric lesions using *in vivo* electron spin resonance spectroscopy, Free Radic. Res. 38 (2004) 147–155.
[23] T. Sonta, T. Inoguchi, S. Matsumoto, K. Yasukawa, M. Inuo, H. Tsubouchi, N. Sonoda, K. Kobayashi, H. Utsumi, H. Nawata, *In vivo* imaging of oxidative stress in the kidney of diabetic mice and its normalization by angiotensin II type 1 receptor blocker, Biochem. Biophys. Res. Commun. 330 (2005) 415–422.
[24] A. Hirayama, S. Nagase, A. Ueda, T. Oteki, K. Takada, M. Obara, M. Inoue, K. Yoh, K. Hirayama, A. Koyama, *In vivo* imaging of oxidative stress in ischemia-reperfusion renal injury using electron paramagnetic resonance, Am. J. Physiol. Renal Physiol. 288 (2005) F597–F603.
[25] P. Kuppusamy, H. Li, G. Ilangovan, A.J. Cardounel, J.L. Zweier, K. Yamada, M.C. Krishna, J.B. Mitchell, Noninvasive imaging of tumor redox status and its modification by tissue glutathione levels, Cancer Res. 62 (2002) 307–312.
[26] A. Hirayama, K. Yoh, S. Nagase, A. Ueda, K. Itoh, N. Morito, K. Hirayama, S. Takahashi, M. Yamamoto, A. Koyama, EPR imaging of reducing activity in Nrf2 transcriptional factor-deficient mice, Free Radic. Biol. Med. 34 (2003) 1236–1242.
[27] H. Sano, K. Matsumoto, H. Utsumi, Synthesis and imaging of blood–brain-barrier permeable nitroxyl-probes for free radical reactions in brain of living mice, Biochem. Mol. Biol. Int. 42 (1997) 641–647.
[28] G. Sosnovsky, Z.W. Cai, A study of the Favorskii rearrangement with 3-bromo-4-oxo-2,2,6,6-tetramethylpiperidin-1-oxyl, J. Org. Chem. 60 (1995) 3414–3418.
[29] D.J. Lurie, J.M.S. Hutchison, L.H. Bell, I. Nicholson, D.M. Bussell, J.R. Mallard, Field-cycled proton electron double-resonance imaging of free-radicals in large aqueous samples, J. Magn. Reson. 84 (1989) 431–437.
[30] B.J. Gaffney, C.H. Elbrecht, J.P.A. Scibilia, Enhanced sensitivity to slow motions using ^{15}N-*nitroxide* spin labels, J. Magn. Reson. 44 (1981) 436–446.
[31] S. Matsumoto, H. Utsumi, T. Aravalluvan, K. Matsumoto, A. Matsumoto, N. Devasahayam, A.L. Sowers, J.B. Mitchell, S. Subramanian, M.C. Krishna, Influence of proton T_1 on oxymetry using Overhauser enhanced magnetic resonance imaging, Magn. Reson. Med. 54 (2005) 213–217.
[32] D.J. Lurie, Proton-electron double resonance imaging, in: L.J. Berlinear (Ed.), *In vivo* EPR (ESR) Theory and Application, Kluwer Academic/Plenum Publishers, New York, 2003, pp. 547–578.
[33] D. Grucker, T. Guiberteau, B. Eclancher, J. Chambron, R. Chiarelli, A. Rassat, G. Subra, B. Gallez, Dynamic nuclear-polarization with nitroxides dissolved in biological-fluids, J. Magn. Reson. 106 (1995) 101–109.
[34] K. Yamada, I. Yamamiya, H. Utsumi, *In vivo* detection of free radicals induced by diethylnitrosamine in rat liver tissue, Free Radic. Biol. Med. 40 (2006) 2040–2046.
[35] H. Utsumi, K. Yasukawa, T. Soeda, K.I. Yamada, R. Shigemi, T. Yao, M. Tsuneyoshi, Non-invasive mapping of reactive oxygen species by *in vivo* electron spin resonance spectroscopy in indomethacin-induced gastric ulcers in rats, J. Pharmacol. Exp. Ther. 317 (2006) 1–8.
[36] A.H. Beth, R.C. Perkins, S.D. Venkataramu, D.E. Pearson, C.R. Park, J.H. Park, L.R. Dalton, Advantages of deuterium modification of nitroxide spin labels for biological electron-paramagnetic-resonance studies, Chem. Phys. Lett. 69 (1980) 24–28.
[37] L.A. Dalton, J.L. Monge, L.R. Dalton, A.L. Kwiram, Molecular and applied modulation effects in electron-electron double resonance. III. Bloch equation analysis for inhomogeneous broadening, Chem. Phys. 6 (1974) 166–182.